

# Separating, transitional flow affected by various inflow oscillation regimes

J. G. Wissink\*

(Received 13 November 2004, revised 25 February 2005)

## Abstract

Consider the direct numerical simulations of laminar separation bubble flow with oscillating oncoming flow. We explore the influence of the amplitude and the period of the inflow oscillation on the dynamics of the separation bubble. The oscillating inflow causes the location of separation and the location of transition to alternately move upstream and downstream. For all simulations, in every period a new separation bubble is formed as the inflow decelerates. The growth-rate of the triggered Kelvin–Helmholtz instability depends on both the amplitude and the period of the inflow-oscillation.

## Contents

### 1 Introduction

C118

---

\*Institute for Hydromechanics, University of Karlsruhe, Karlsruhe, GERMANY.  
<mailto:wissink@ifh.uni-karlsruhe.de>

See <http://anziamj.austms.org.au/V46/CTAC2004/Wiss> for this article, © Austral. Mathematical Soc. 2005. Published April 6, 2005. ISSN 1446-8735

<i>Contents</i>	C118
<b>2 Results</b>	<b>C121</b>
<b>3 Conclusions</b>	<b>C131</b>
<b>References</b>	<b>C132</b>

## 1 Introduction

In the presence of a strong enough adverse pressure gradient, a laminar boundary layer over a flat plate will separate. The separated boundary layer (shear layer) is very unstable and will usually undergo rapid transition to turbulence. Previous Direct Numerical Simulations (DNS) of Laminar Separation Bubble (LSB) flow with constant free stream have been performed by Alam and Sandham [1], Maucher et al. [2], Spalart and Strelets [3] and Wissink and Rodi [4]. To generate an adverse pressure gradient, required for the formation of a LSB, both Alam and Sandham as well as Spalart and Strelets used suction through the upper boundary, Maucher et al. applied a special boundary condition for the free-stream velocity and Wissink and Rodi employed the special shape of the upper wall (see also Figure 1). By explicitly introducing disturbances into the boundary layer prior to separation, Alam and Sandham observed that the separated shear layer undergoes transition via oblique modes and  $\Lambda$ -vortex induced breakdown. They also showed that the LSB flow becomes absolutely unstable when the reverse flow exceeds 15–20% of the local free-stream velocity. As Alam and Sandham, Maucher et al. explicitly added disturbances to the attached laminar boundary layer as they focused on the early stages of transition. Both Spalart & Strelets and Wissink & Rodi relied on small numerical round-off error present in any numerical simulation to trigger natural modes. They detected a Kelvin–Helmholtz (KH) instability, characterized by a quasi-periodic shedding of vortices from the separated boundary layer.

The addition of inflow oscillations induces an oscillating pressure gra-

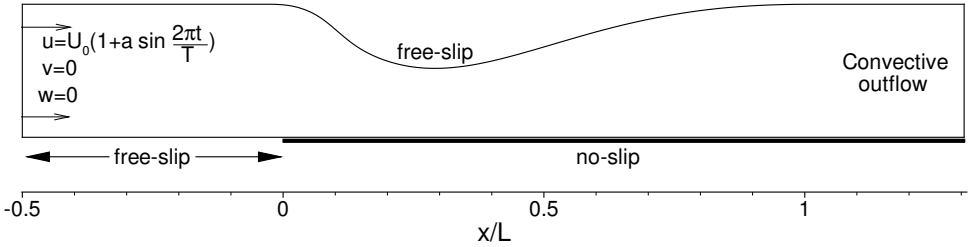


FIGURE 1: Spanwise slice through the computational domain

dient which causes the location of separation to move back and forth. To be able to perform a detailed study, several Direct Numerical Simulations (DNS) of separating flow over a flat plate with oscillating inflow have been performed. The computational domain is illustrated in Figure 1. The adverse pressure gradient is induced by the special shape of the upper wall. In the spanwise direction periodic boundary conditions are employed, while at the outlet a convective outflow boundary condition is used. Along the upper boundary and along the lower boundary for  $x < 0$  a free-slip boundary condition is prescribed. A no-slip boundary condition is employed along the lower boundary for  $x \geq 0$ . Finally, at the inlet an oscillating flow  $(u, v, w) = U_0(1 + a \sin \frac{2\pi t}{T}, 0, 0)$ , where  $a$  is the amplitude and  $T$  is the period of the inflow, is employed. The Reynolds number of the flow problem,  $\text{Re} = 60\,000$ , is based on the mean inflow velocity  $U_0$  and the length of the flat plate  $L$ , as chosen in companion experiments performed at the Technical University of Berlin.

An overview of the performed simulations is provided in Table 1. Both the amplitude  $a$  and the period  $T$  of the inflow oscillation were varied in order to be able to study their influence on the dynamics of the LSB. In all simulations, the primary instability-mechanism for the transition to turbulence was found to be a two-dimensional KH instability of the separated shear layer which was triggered by the inflow oscillation. The KH instability caused the shear layer

TABLE 1: Overview of the simulations performed

Simulation	Spanwise size	grid	$a$	$T$
A	$0.12 L$	$966 \times 226 \times 128$	0.20	$0.61 L/U_0$
B	$0.08 L$	$1286 \times 310 \times 128$	0.10	$0.30 L/U_0$
C	$0.12 L$	$966 \times 226 \times 128$	0.05	$0.30 L/U_0$
D	$0.12 L$	$966 \times 226 \times 128$	0.05	$0.15 L/U_0$

to roll up. Inside the rolled up shear layer, entrained disturbances triggered elliptic instabilities which lead to a rapid transition to fully three-dimensional (3D) turbulence [5, 6].

The computations were performed on the IBM SP-SMP supercomputer in Karlsruhe using up to 128 processors and  $51 \times 10^6$  grid points. To optimize load balancing, the computational domain was subdivided into subdomains of equal size which were each assigned to their own unique processor. Communication between processors was performed through the standard Message Passing Interface (MPI) protocol. The 3D, incompressible Navier–Stokes equations were discretised using a finite-volume approach, employing a central, second-order accurate discretisation in space, combined with a three-stage Runge–Kutta method for the time-integration.

Phase-averaging was performed by subdividing each period into 256 equal phases  $\phi = 0, \frac{1}{256}, \dots, \frac{255}{256}$  at which statistics were gathered. To speed up the convergence of the statistics, phase-averaging was combined with averaging in the homogeneous spanwise direction. In each simulation, phase-averaging has been performed during at least six non-dimensional time-units  $L/U_0$ . Notation:  $\langle f \rangle$  is the phase-averaged signal of the quantity  $f$ .

In Section 2, a detailed comparative study of the dynamics of LSB flow under different inflow oscillation regimes is presented using both instantaneous flow fields and phase-averaged statistics. A further discussion of the results and the conclusions is in Section 3.

## 2 Results

In this section, some key results of the simulations listed in Table 1 will be presented. The aim is to elucidate the influence of the amplitude and period of the oscillating inflow on the dynamics of a laminar separation bubble flow.

Figures 2 and 3 shows the phase-averaged location of separation during two periods as a function of phase  $\phi$ . Separation is identified by grey contours, corresponding to negative values of the friction velocity  $\langle u_\tau \rangle = \sqrt{\nu \partial \langle u \rangle / \partial y}$ . Each plot, corresponding to one of the Simulations A-D (see Table 1), shows the formation of a new separation bubble as the inflow starts to—or is about to start to—decelerate ( $\phi \approx 0.25, 1.25$ ). As the inflow decelerates, the separation bubble grows in both the upstream and downstream direction. As the inflow is about to accelerate ( $\phi \approx 0.75 \bmod 1$ ), a large roll of re-circulating flow—identified by label ‘I’—is shed. The remainder of the separation bubble—identified by label ‘II’—is only visible in the graphs corresponding to Simulations A and B. While in Simulation A parts of separation bubbles stemming from different periods never merge, in Simulation B the newly formed separation bubble is found to merge with Region II from the bubble that was formed during the previous period.

The maximum streamwise extent of the bubble is observed to depend on the period  $T$ , which determines the duration of the deceleration period, and the inflow amplitude  $a$ , which determines the strength of the deceleration. Compared to Simulation C, the larger inflow oscillation-amplitude that is employed in Simulation B induces a stronger deceleration for  $0.25 < \phi < 0.75$ . As a consequence, in Simulation B one can observe a faster growth of the separation bubble during the initial phases of inflow-deceleration as well as a periodic recirculation ”revival” of Region II. Also, the increased triggering of the KH instability in Simulation B is found to lead to a faster roll-up of the shear layer—illustrated by the fact that the maximum reverse flow (labeled ‘M’) is reached at an earlier phase—and to promote the subsequent destruction of the old separation bubble (Region I) as it is convected down-

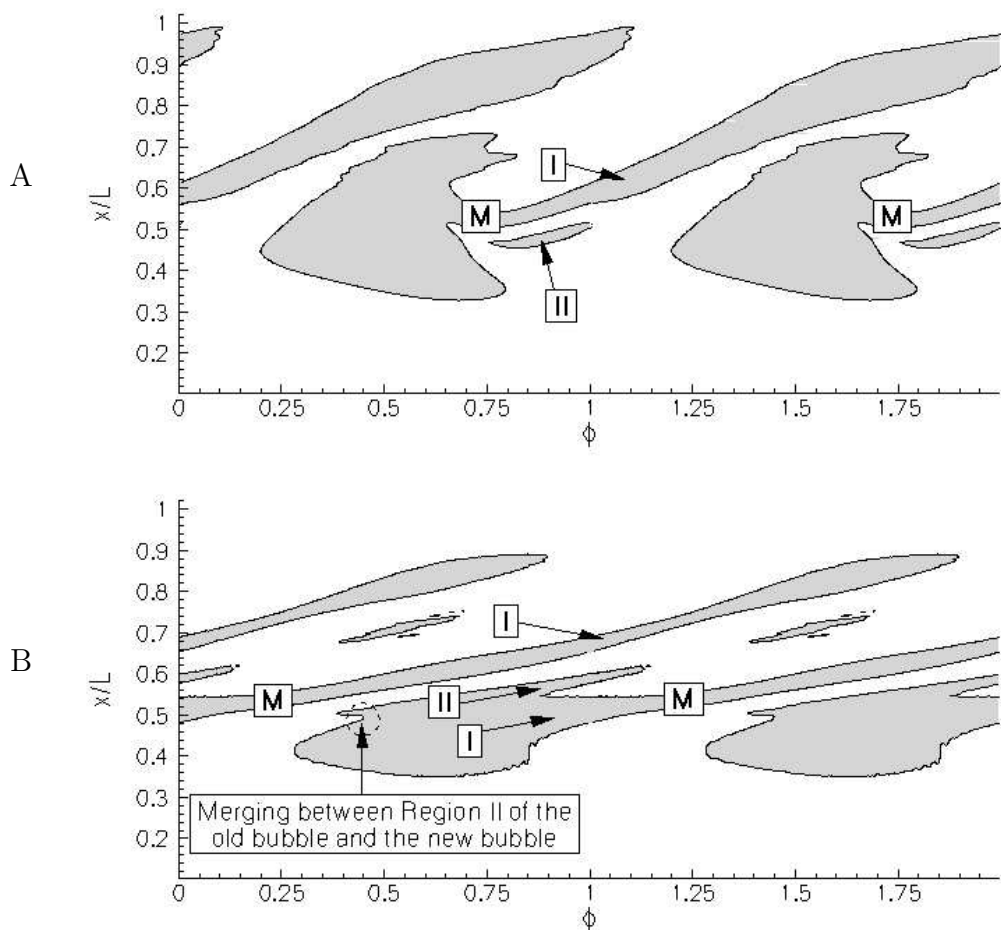


FIGURE 2: Space-time plot showing two periods of the phase-averaged location of separation as a function of phase  $\phi$  for Simulations A and B.

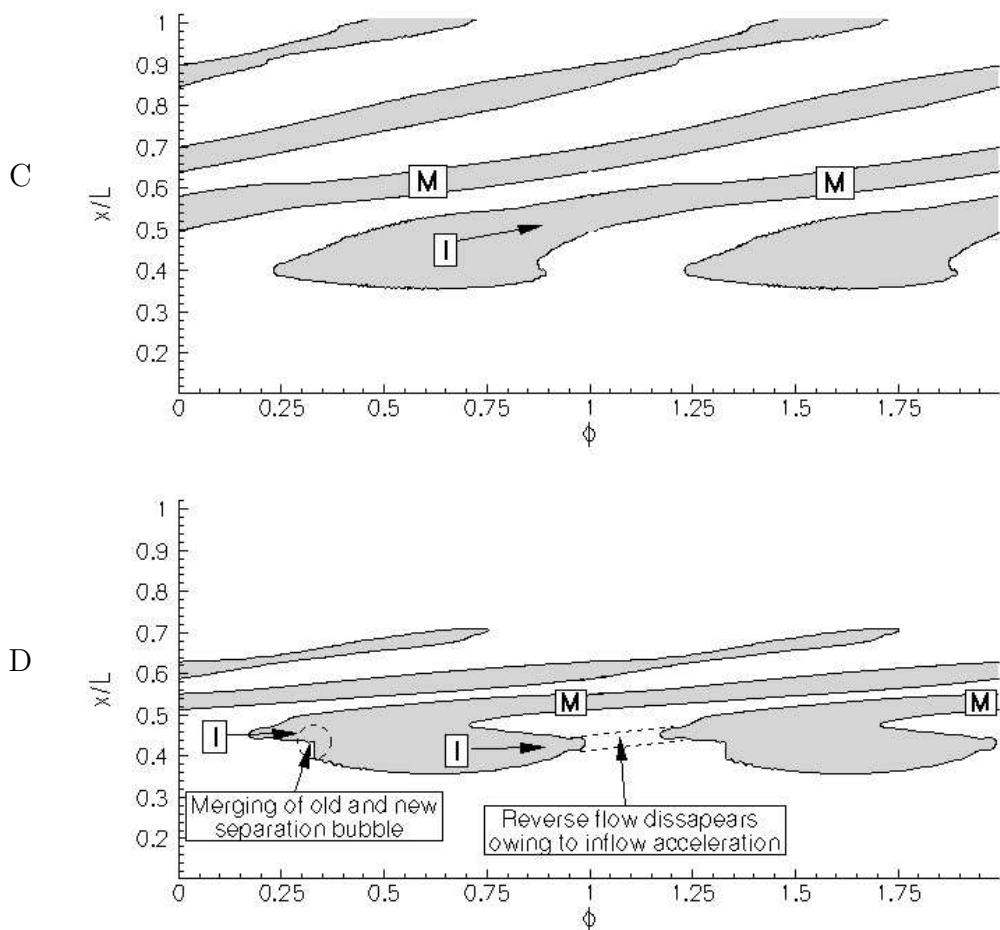


FIGURE 3: Space-time plot showing two periods of the phase-averaged location of separation as a function of phase  $\phi$  for Simulations A and B.

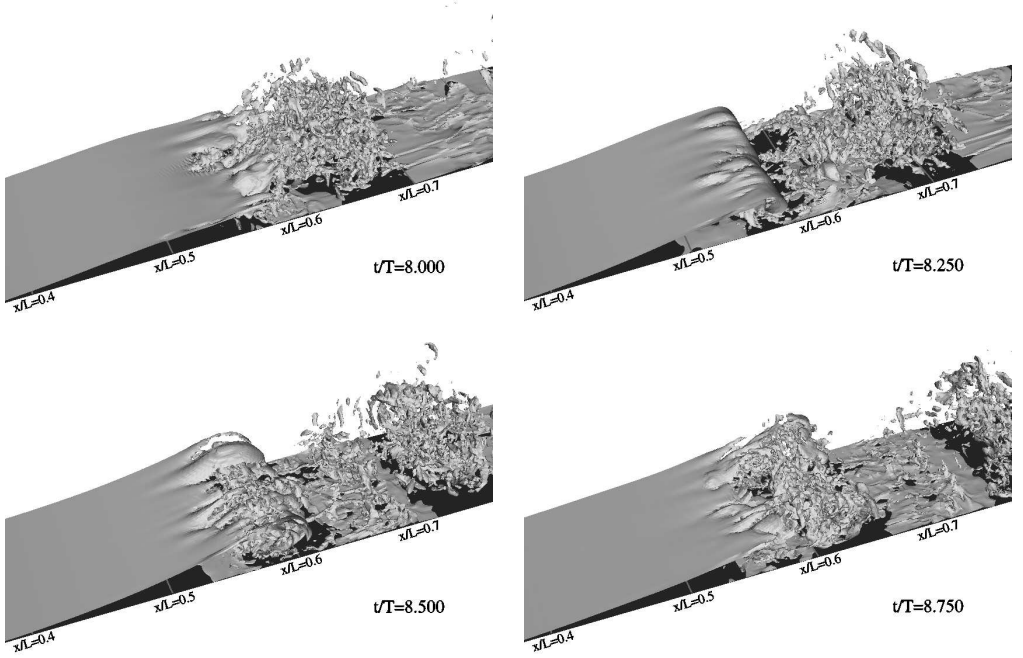


FIGURE 4: Series of snapshots showing the instantaneous spanwise vorticity in Simulation C.

stream (compare Simulations B and C in Figures 2–3).

The effect of decreasing the inflow-oscillation period  $T$  is studied by comparing the results of Simulations C and D in Figure 3. The decreased period in Simulation D is observed to result in a merger of Region I of the old bubble with the newly formed bubble. Also, the relatively small period does not allow enough time for the recirculating flow associated with the KH instability to become very strong. As a result, the accelerating inflow—which displaces the velocity field inside the channel—is strong enough to make the recirculating region invisible for  $1 < \phi < 1.2$ . As in Simulations B and C, the maximum reverse flow is reached in the period following the period in which the bubble was formed.

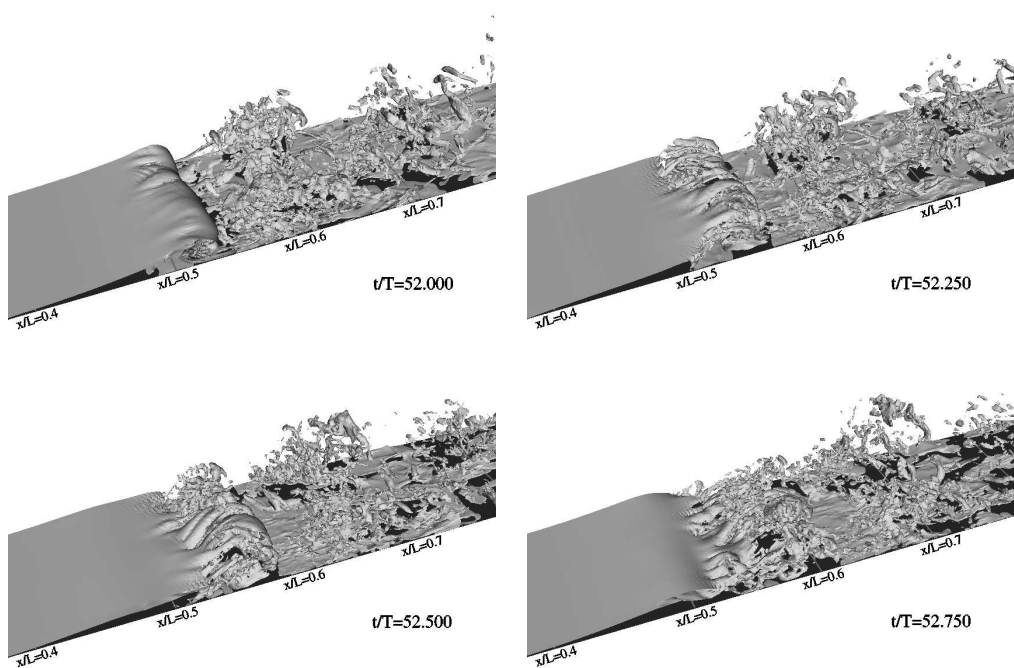
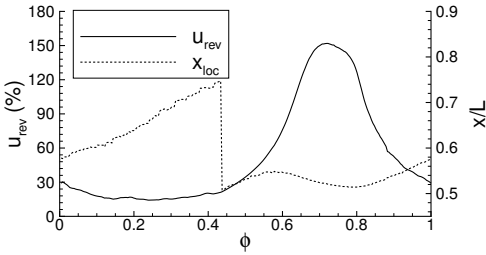


FIGURE 5: Series of snapshots showing the instantaneous spanwise vorticity in Simulation D.

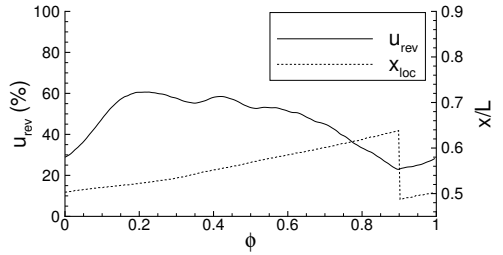
Figures 4–5 shows a series of snapshots of the instantaneous spanwise vorticity, illustrating the evolution of the separation bubble in Simulations C (Figure 4) and D (Figure 5) during one inflow-oscillation period. In Simulation C a small area of becalmed flow is found to be present in between the remains of separation bubbles formed at subsequent periods. For both simulations, the snapshots clearly illustrate the roll up of the separated boundary layer and the subsequent shedding of this spanwise roll of re-circulating flow. As soon as the roll is shed, the re-circulating flow very quickly turns turbulent [3, 5, 6]. The large spanwise rolls of recirculating flow correspond to the Regions I as displayed in Figures 2–3. Owing to the decreased period in Simulation D, compared to Simulation C the size of the separation bubble decreases.

In Figure 6 the magnitude of the phase-averaged reverse flow—as a percentage of the local free-stream velocity—and its streamwise location have been plotted as a function of phase for all simulations. In Simulations B–D the maximum reverse flow reaches values above 20% of the free-stream velocity for all phases (see Figure 6b–d). Consequently, the flow in Simulations B–D is absolutely unstable [1] and self-sustained turbulence can exist for all phases. In Simulation A the maximum reverse flow is above 20%, and is thus absolutely unstable, for  $0 \leq \phi < 0.07$  and  $0.45 < \phi \leq 1$  (see Figure 6a). The sudden jumps in the graphs of the location of maximum reverse flow are a consequence of the reverse flow of a newly formed separation bubble growing stronger than the reverse flow of the bubble formed during the preceding period.

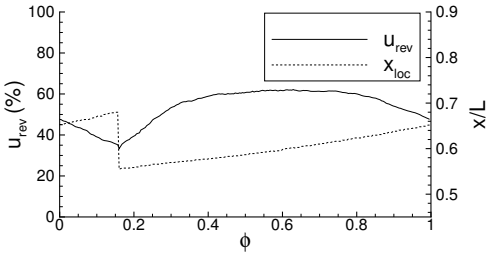
Making use of the information about the location of the separation bubbles provided in Figures 2–3, it is possible to determine the time interval  $\Delta t$  between the appearance of a new separation bubble and the phase at which the re-circulating flow reaches its maximum. As already noted before, the location of this absolute maximum is identified by the label ‘M’ in Figures 2–3. The first appearance of the separation bubble is around  $\phi = 0.25$ . In Simulation A, the maximum reverse flow is reached at  $\phi = 0.74$ , giving



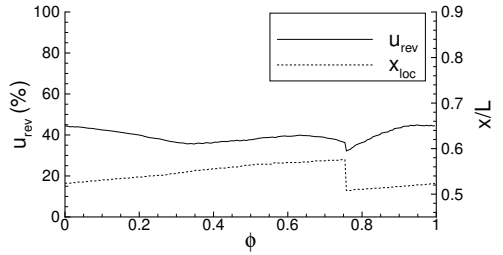
(a)



(b)



(c)



(d)

FIGURE 6: Phase-averaged maximum reverse flow as a percentage of the local free-stream velocity and location of maximum reverse flow both as a function of phase.

$\Delta t = 0.49T \approx 0.30L/U_0$ . In Simulation B, the maximum is reached at  $\phi = 1.22$ , giving  $\Delta t = 0.29L/U_0$ . The reverse flow in Simulation C is maximum at  $\phi \approx 1.60$  such that  $\Delta t = 0.40L/U_0$ , while in Simulation D the maximum is reached at  $\phi \approx 1.92$  giving  $\Delta t = 0.25L/U_0$ . This again confirms that a smaller amplitude of the inflow oscillation results in a slower development of the KH instability which is responsible for the roll-up of the shear layer (compare Simulation B to Simulation C). Decreasing the inflow oscillation period—while keeping its amplitude constant—on the other hand is observed to result in a stronger triggering of the KH instability (compare Simulation D to Simulation C).

The latter is explained by Figures 7–8. In these figure, for both Simulations C and D, the frequency spectra of the  $v$ -velocities at four points  $P_1, \dots, P_4$ , located at midspan is shown. The points are identified in the lower graphs showing contours of the mean spanwise vorticity. In Simulation C, the first peak in the spectrum at  $f = 3.33U_0/L$  corresponds to the inflow oscillation frequency. The most amplified mode of the KH instability is found to be the second harmonic of this fundamental frequency  $f_{\max} = 6.67U_0/L$ . In Simulation D, the inflow oscillation frequency  $f = 6.67$  is identical to the most amplified mode of the KH instability. This direct triggering of the most unstable KH mode results in a rapid growth of the KH instability and explains the stronger triggering of the KH instability in Simulation D as compared to Simulation C.

Above, it was shown that the maximum streamwise extent of the separation bubble depends mostly on the inflow oscillation period. Increasing the amplitude of the oscillation, results in a stronger triggering of the KH instability which promotes the decay of the separation bubble. Finally, a direct triggering of the most unstable KH mode by an appropriate choice of the inflow oscillation period was also found to significantly promote the decay of the LSB.

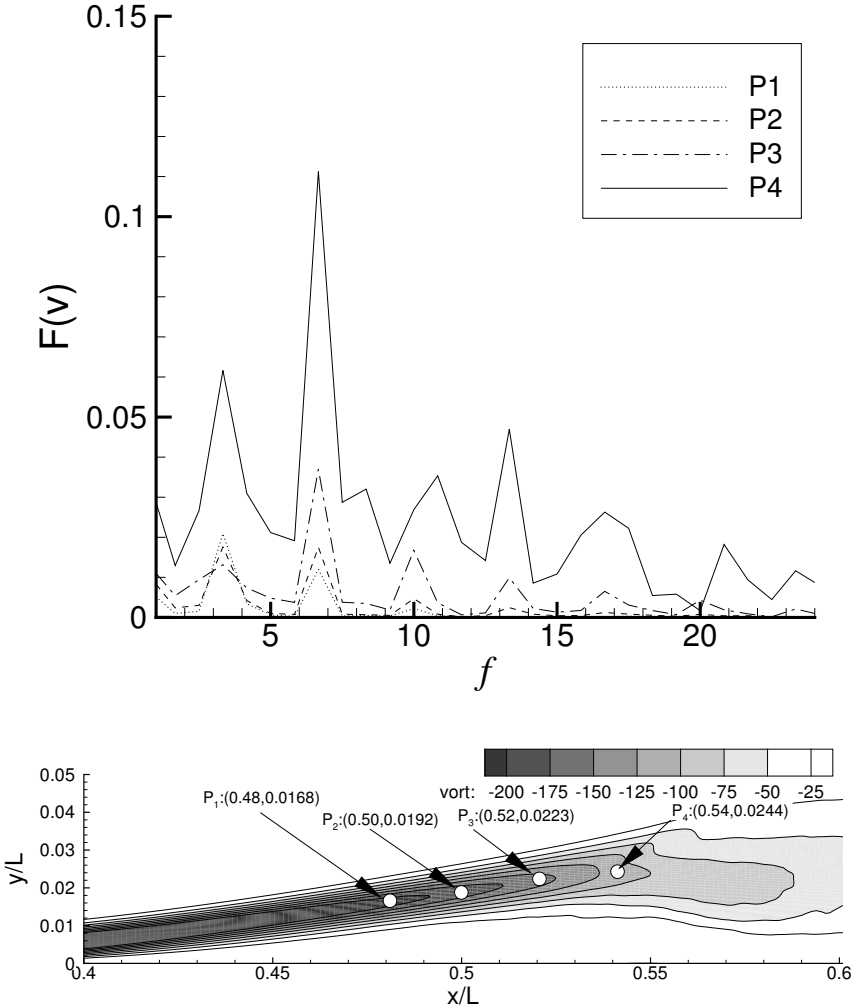


FIGURE 7: Frequency spectra of the instantaneous  $v$ -velocity at  $P_1, P_2, P_3, P_4$ .  $P_1, \dots, P_4$  are identified in the lower graphs, showing contours of the time-averaged spanwise vorticity in Simulation C.

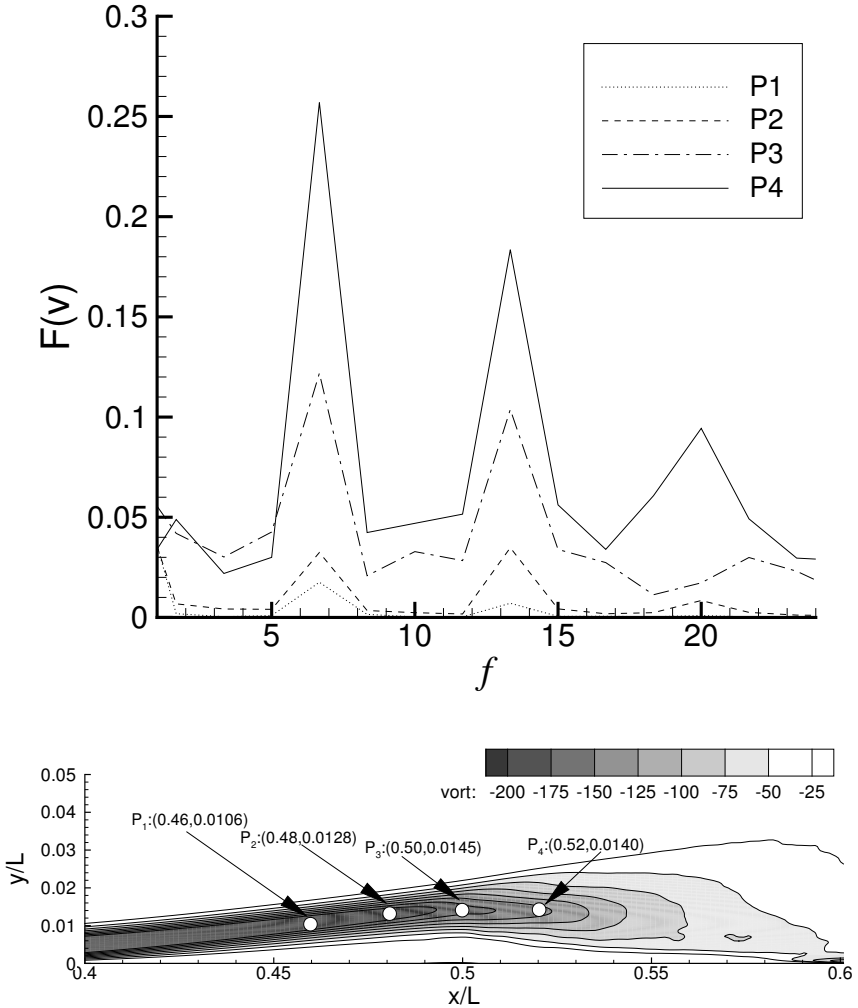


FIGURE 8: Frequency spectra of the instantaneous  $v$ -velocity at  $P_1, P_2, P_3, P_4$ .  $P_1, \dots, P_4$  are identified in the lower graphs, showing contours of the time-averaged spanwise vorticity in Simulation D.

### 3 Conclusions

Several DNS of laminar separation bubble flow with oscillating oncoming flow were performed. By varying both the amplitude and the period of this oscillation, its influence on the dynamics of the laminar separation bubble was studied. The results presented above lead to the following conclusions:

- In each of the simulations a new separation bubble was found to be formed around  $\phi = 0.25$ , corresponding to the onset of inflow deceleration.
- If the oscillation period is sufficiently long, the newly formed separation bubble will never merge with the remainder of bubbles formed during previous periods.
- Increasing the amplitude of the inflow-oscillation while keeping its period constant, leads to a stronger triggering of the KH instability which manifests itself by a faster roll-up of the separated shear layer.
- Choosing the period of the inflow-oscillation to match the one of the most unstable KH mode also leads to a faster roll-up of the separated shear-layer.
- In all simulations, the very fast transition to turbulence is found to take place inside the rolled up shear layer.
- Except for a brief period around  $\phi = 0.25$  in Simulation A, the maximum reverse flow in all simulations reaches values in excess of 20% of the free-stream velocity. According to Alam and Sandham [1] such flows are absolutely unstable and self-sustained turbulence can exist.

**Acknowledgment:** The author thanks the German Research Foundation (DFG) for funding this research.

## References

- [1] M. Alam and N. D. Sandham. Direct Numerical Simulation of 'short' laminar separation bubbles with turbulent reattachment. *J. Fluid Mech.*, 410:1–28, 2000. [URL link](#). C118, C126, C131
- [2] U. Maucher and U. Rist and M. Kloker and S. Wagner. DNS of laminar-turbulent transition in separation bubbles. In E. Krause and W. Jäger, editors, *High-Performance Computing in Science and Engineering*, Springer, 2000. C118
- [3] P. R. Spalart and M. Kh. Strelets. Mechanisms of transition and heat transfer in a separation bubble. *J. Fluid Mech.*, 403:329–349, 2000. [URL link](#). C118, C126
- [4] J. G. Wissink and W. Rodi. DNS of transition in a laminar separation bubble. In I. P. Castro and P.E. Hancock, editors, *Advances in Turbulence IX, proceedings of the Ninth European Turbulence Conference*, CIMNE, 2002. C118
- [5] J. G. Wissink and W. Rodi. DNS of a laminar separation bubble in the presence of oscillating flow. *Flow, Turbulence and Combustion*, 71:311–331, 2003. C120, C126
- [6] J. G. Wissink and V. Michelassi and W. Rodi. Heat transfer in a laminar separation bubble affected by oscillating external flow. *Int. J. of Heat and Fluid Flow*, 25:729–740, 2004. <http://dx.doi.org/10.1016/j.ijheatfluidflow.2004.04.005> C120, C126